

A blueprint for truncation resonance placement in elastic periodic lattices with unit cell asymmetry

Hasan B. Al Ba'ba'a,^{1,2} Hosam Yousef,² and Mostafa Nouh^{2,3, a)}

¹⁾Department of Mechanical Engineering, Union College, Schenectady, NY 12308

²⁾Department of Mechanical and Aerospace Engineering, University at Buffalo (SUNY), Buffalo, NY 14260

³⁾Department of Civil, Structural and Environmental Engineering, University at Buffalo (SUNY), Buffalo, NY 14260

(Dated: 27 November 2023)

Elastic periodic lattices act as mechanical filters of incident vibrational loads. By and large, they forbid wave propagation within bandgaps and resonate outside them. However, they often encounter ‘truncation resonances’ inside bandgaps when certain conditions are met. This study provides an all-encompassing blueprint for the design and selective placement of truncation resonances in elastic periodic lattices, integrating all factors that play a role in the onset of truncation resonances and shaping the finite lattice’s response, from unit cell configuration, mass and stiffness contrasts, to types and symmetry of boundary conditions.

At their very core, elastic periodic lattices are effective mechanical filters of incident excitations. Lattices comprised of a sequence of two or more alternating layers exhibit Bragg scattering preventing vibrations within selected frequency ranges (bandgaps) from being transmitted through the material^{1,2}. They represent a class of phononic crystals, owing to the similarity between the periodic array of lumped spring-mass elements and the ordered arrangement of atoms in a crystalline material^{3,4}. The majority of structural resonances associated with such lattices fall within its propagation frequencies or ‘pass bands’. Yet, finite lattices are known to encounter natural frequencies which avert these pass bands and end up inside bandgaps, forcing a unique combination of high-amplitude deformations emblematic of resonances and an exponential spatial attenuation of the incident wave towards the bulk of the medium⁵. The result is a localized mode where a large amount of energy is confined to one edge of the structure, opening up new avenues of research in the field of wave focusing and guidance. Among other names, these unique resonances have been referred to as truncation and bandgap resonances, given their direct relation to the location at which an infinite array of unit cells is truncated to form a finite one and their existence within bandgap regions.

Despite the widespread usage of truncation resonances in engineering applications (topological insulation⁶⁻⁸, flow control^{9,10}, and aerodynamic laminar-to-turbulent transition delay¹¹, to name a few), the study of their existence criteria has been less prevalent. In 2011, Davis *et al.* examined anomalous truncation resonances appearing in periodic flexural beams¹². Almost a decade later, Al Ba'ba'a *et al.* formalized the theory of truncation resonance origination in solid continua, establishing the role of symmetry in both unit cell choice and boundary conditions¹³. Rosa *et al.* further developed the topological origins associated with some truncation resonances in continuous structures¹⁴. Additional studies

have shed light on different aspects of truncation resonances, for example, those exhibited by locally resonant metamaterials¹⁵, bandgap resonances which accompany defect modes^{16,17}, and the use of such resonances to manipulate Lamb¹⁸ and surface acoustic waves¹⁹. Despite the presence of some analogies, elastic lattices of discrete atoms have been known to behave differently under similar conditions and therefore merit their own framework. In 2017, Al Ba'ba'a *et al.* derived the existence criteria of truncation resonances in elastic lattices with two periodic atoms as well as uniform lattices with a periodic elastic foundation²⁰, and later generalized this analysis to polyatomic²¹ and inertially amplified lattices²². Bastawrous and Hussein extended these criteria to general boundary conditions as well as lattices with end masses²³. In this work, we present a blueprint for the design and selective placement of truncation resonances in elastic periodic lattices. The paradigm presented here absorbs all the pertinent factors that play a role in the onset of truncation resonances and shape the dynamic response of a finite lattice, spanning unit cell configuration, mass and stiffness contrasts, as well as types and symmetry of boundary conditions, and integrates them to delineate the theory of truncation resonances in monatomic and diatomic lattices. In doing so, we also demonstrate how the location at which deformations are confined in truncation resonance edge modes are rooted in the lattice’s constitutive symmetry parameters.

Monatomic lattice. Consider a monatomic lattice with stiffness k , mass m , and u_i denoting the displacement of the i^{th} mass. Owing to its periodicity, the building block of the infinite lattice (i.e., the unit cell) can be defined in an infinite number of ways. Using a symmetry parameter δ , the lumped masses contained within a given unit cell can be parameterized as $m_{\pm} = \frac{m}{2}(1 \pm \delta)$, where m_{\pm} represents the masses connected to both ends of the spring k , as depicted in Fig. 1(a). Consequently, the motion equations of an isolated unit cell simplify to

$$(1 - \delta)\ddot{u}_i + 2\omega_0^2(u_i - u_{i+1}) = 2f_L/m \quad (1a)$$

$$(1 + \delta)\ddot{u}_{i+1} + 2\omega_0^2(u_{i+1} - u_i) = 2f_R/m \quad (1b)$$

^{a)}Corresponding author: mnouh@buffalo.edu

where $\ddot{(\)}$ is an acceleration, $\omega_0 = \sqrt{k/m}$, and $f_{L,R}$ are the forces on both sides. Upon assuming a harmonic solution and casting these equations in a transfer matrix format³, the state vectors at the i^{th} and $i + 1^{\text{th}}$ nodes of the lattice can be related via $\{u_{i+1} \ \epsilon_{i+1}\}^T = \mathbf{T} \{u_i \ \epsilon_i\}^T$, where $\epsilon_i = 2f_L/k$, $\epsilon_{i+1} = -2f_R/k$, and the transfer matrix \mathbf{T} is given by

$$\mathbf{T} = \begin{bmatrix} 1 - \frac{1}{2}(1 - \delta)\Omega^2 & -\frac{1}{2} \\ \frac{1}{2}\Omega^2(4 - (1 - \delta^2)\Omega^2) & 1 - \frac{1}{2}(1 + \delta)\Omega^2 \end{bmatrix} \quad (2)$$

where $\Omega = \omega/\omega_0$. The wave dispersion relation is defined as $\text{tr}(\mathbf{T}) = 2\cos(q)$, which amounts to $\Omega = \sqrt{2(1 - \cos(q))}$ with q being a nondimensional wavenumber. As one might expect, we find the dispersion relation to be indifferent to the unit cell choice, as evident by its independence of the symmetry parameter δ ¹³.

Once an infinite lattice is truncated to a finite size, δ plays an instrumental role in the ensuing lattice behavior. The states at the two lattice ends can be related via \mathbf{T}^n , where n is the number of cells in the finite lattice. An expression for \mathbf{T}^n can be found as follows²⁴

$$\mathbf{T}^n = \frac{\cos(nq)}{2\cos(q)} (\mathbf{T} + \mathbf{T}^{-1}) + \frac{\sin(nq)}{2\sin(q)} (\mathbf{T} - \mathbf{T}^{-1}) \quad (3)$$

in which the four matrix elements are henceforth identified as t_{11n} (top left), t_{12n} (top right), t_{21n} (bottom left), and t_{22n} (bottom right), given by

$$t_{11n} = \cos(nq) + \frac{\sin(nq)}{2\sin(q)}\delta\Omega^2 \quad (4a)$$

$$t_{12n} = -\frac{\sin(nq)}{2\sin(q)} \quad (4b)$$

$$t_{21n} = \Omega^2(4 - (1 - \delta^2)\Omega^2) \frac{\sin(nq)}{2\sin(q)} \quad (4c)$$

$$t_{22n} = \cos(nq) - \frac{\sin(nq)}{2\sin(q)}\delta\Omega^2 \quad (4d)$$

The resonances of an unconstrained (i.e., free-free) finite lattice are captured by the characteristic equation $t_{21n} = 0$, which gives three sets of natural frequencies: (i) $\Omega = 0$ (rigid body mode), (ii) $\Omega = 2(1 - \delta^2)^{-\frac{1}{2}}$, and (iii) a group of $n - 1$ frequencies which can be computed by setting $q = r\pi/n$ in the lattice's dispersion relation, with $r = 1, 2, \dots, n - 1$. Groups (i) and (iii) represent n natural frequencies that fall within the propagating zone of the monatomic lattice and satisfy the dispersion relation. In other words, each of these frequencies corresponds to a mode shape generating an $[\Omega, q]$ point which lies on the lattice's dispersion curve, as shown in Fig. 1(b). The natural frequency given by (ii), however, is larger than the cut-off frequency of the lattice at $\Omega = 2$ for any non-zero values of $\delta \in (-1, 1)$. It coincides with the cut-off frequency at $\delta = 0$ and rapidly approaches infinity as $|\delta| \rightarrow 1$. This natural frequency indicates a unique resonance which lies outside the lattice's pass band and is therefore unrecognizable by the dispersion analysis of

the single unit cell. Instead, it is perceived as a direct outcome of the finite lattice's parameters, i.e., size and boundary conditions. Since these parameters culminate from trimming an infinite lattice to form a finite one, this natural frequency is customarily referred to as a 'truncation resonance'¹³. The leftmost panel of Fig. 1(b) shows the dispersion diagram of a monatomic lattice with a unit cell configuration corresponding to $\delta = \pm 1/\sqrt{2}$. Since it consists of a repeated array of single degree-of-freedom unit cells, the monatomic lattice has one wave mode described by a single dispersive branch which ends at the edge of the irreducible Brillouin zone ($q = \pi$) and is followed by an unbounded stop band starting at the cut-off frequency ($\Omega = 2$). Shown in the same figure are the $n + 1 = 11$ natural frequencies of a finite free-free monatomic lattice constructed from $n = 10$ unit cells of the same configuration. As can be seen, a truncation resonance at $\Omega = \sqrt{8}$, as obtained from group (ii), can be spotted in the lattice's stop band. All natural frequencies are further confirmed via conventional modal analysis of the lattice's full mass and stiffness matrices. The eleven eigenfrequencies (cross markers) perfectly match the analytical natural frequencies (circular markers) obtained from all three groups.

The natural frequencies of a fixed-fixed finite lattice are effectively a subset of the free-free resonances, and are therefore fairly straightforward. They are obtained by setting $t_{12n} = 0$, which gives a set of $n - 1$ frequencies that are identical to those found in group (iii) of the free-free system. Notably, the fixed-fixed lattice has two natural frequencies less than its free-free counterpart due to the zero-displacement constraint on the masses at both ends, effectively eliminating them from the dynamical model as depicted in the schematic of Fig. 1(a). Physically speaking, one of these two natural frequencies is the rigid body mode at $\Omega = 0$ which no longer exists once the lattice is anchored to fixed walls at both ends. The other one is the truncation resonance which also no longer exists in the fixed-fixed system since it is solely a function of δ . The middle panel of Fig. 1(b) shows the dispersion diagram and natural frequencies obtained for the same parameters used in the free-free case, namely $\delta = \pm 1/\sqrt{2}$ and $n = 10$. The results confirm the lack of a truncation resonance in the fixed-fixed lattice. Since the dispersion curve is obtained from a unit cell analysis, it is independent of the finite lattice's boundary conditions as evident by the identical dispersion diagram obtained for both systems. Finally, it is important to note that the wave propagation profile associated with a truncation resonance is an edge mode, where energy is confined to one end of the lattice and is unable to infiltrate the elastic medium since the frequency lies outside of its pass band^{13,14}. In the monatomic lattice, these localizations take place at the edge with the 'lighter' mass. As a result, a negative δ results in an energy localization at the right end of the lattice, while a positive δ induces localization at its left end. This symmetry effect is captured in the rightmost panel of Fig. 1(b).

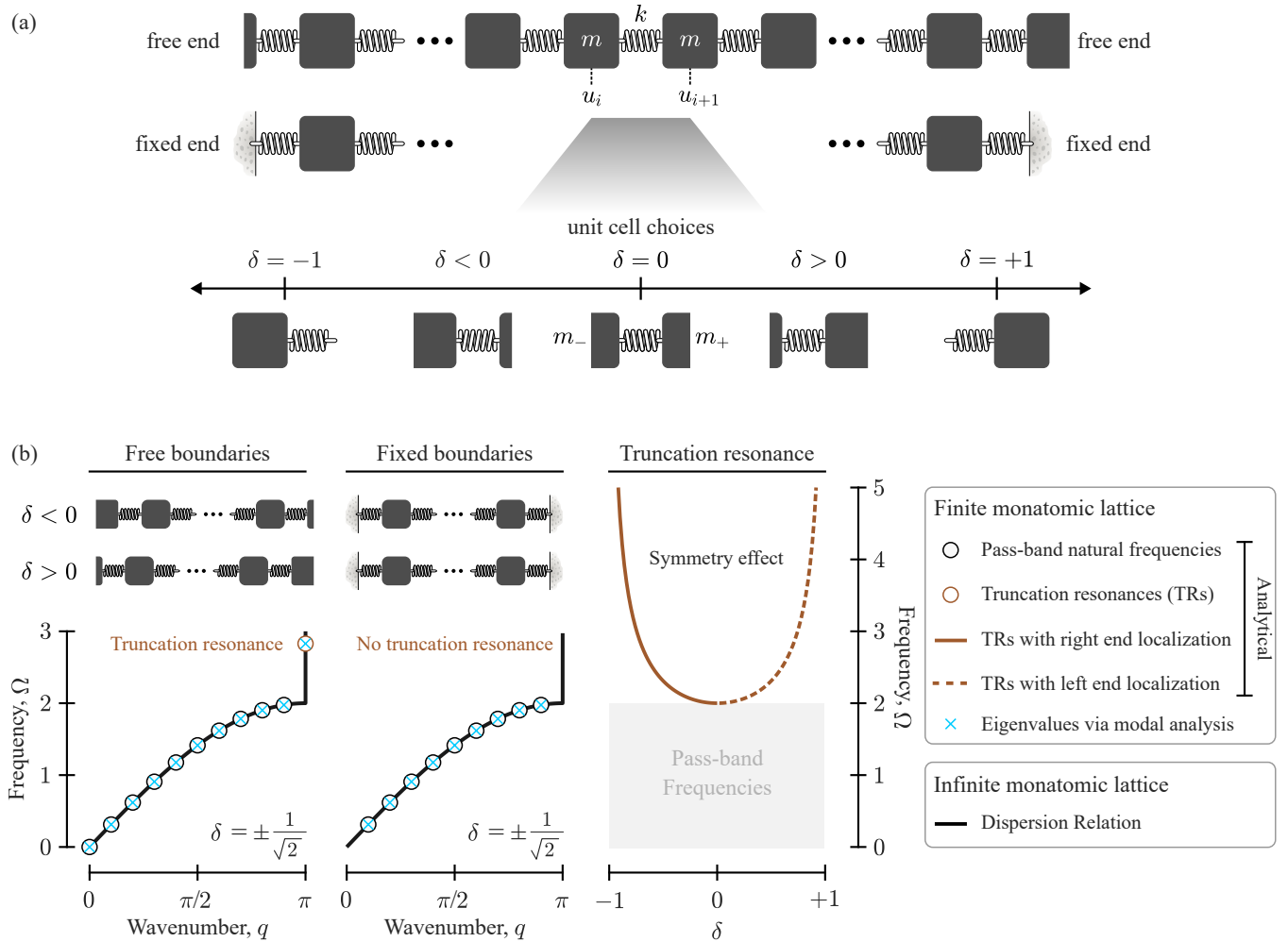


FIG. 1. **Monatomic lattice.** (a) Schematic diagram of a finite monatomic lattice comprised of a series of identical masses m connected via identical springs k , subject to free and fixed boundary conditions. Owing to its periodicity, the building block (unit cell) of the monatomic lattice can be defined in an infinite number of ways using the single symmetry parameter δ , where $-1 \leq \delta \leq 1$. While the choice of unit cell does not affect the dispersion relation, a finite lattice shall generally have different end masses whose values depend on the sign and value of δ . A positive δ will result in a heavier portion of the lumped mass ($> m/2$) on the right end of the lattice, and vice versa. $\delta = 0$ denotes a perfectly symmetric unit cell where $m_+ = m_- = m/2$. (b) Natural frequencies of a free-free (left) and fixed-fixed (middle) finite monatomic lattice of $n = 10$ unit cells and $\delta = \pm 1/\sqrt{2}$, superimposed on the dispersion diagram of the infinite lattice. Truncation resonances (TRs) are marked with a circular marker of different color for distinction. One TR appears in the free-free lattice at $\Omega = \sqrt{8}$ while none exist in the fixed-fixed case. The rightmost plot tracks the location of the aforementioned TR as δ varies, showing perfect mirror symmetry about $\delta = 0$. The line style depicts the lattice end associated with the TR's edge mode localization (*solid*: right-end edge mode, $\delta < 0$; *dashed*: left-end edge mode, $\delta > 0$).

The two remaining scenarios, i.e., free-fixed and fixed-free lattices, are indicative of asymmetric boundary conditions and their characteristic equations are given by $t_{11n} = 0$ and $t_{22n} = 0$, respectively. The fact that $t_{11n}(\delta) = t_{22n}(-\delta)$ shows that one of these cases can be obtained from the other by inverting the sign of the symmetry parameter, and makes it sufficient to study either one of them. Let's start by examining a couple of special cases. If $\delta = 0$ (a perfectly symmetric unit cell), both characteristic equations become identical and reduce to $\cos(nq) = 0$, resulting in n pass-band natural frequencies satisfying $q = \frac{2r-1}{2n}\pi$, with $r = 1, 2, \dots, n$. If $\delta = \pm 1$, the free-end mass of the lattice is either 0 or m , and the characteristic equation $t_{22n} = 0$ reduces

to $\cos((2n \mp 1)q/2) = 0$, once again revealing the absence of truncation resonances. However, the pass-band natural frequencies in this case satisfy $q = \frac{2r-1}{2(n \mp 1)}\pi$, with $r = 1, 2, \dots, \varepsilon$, where $\varepsilon = n$ or $n-1$ depending on whether the free-end mass exists or not, respectively. For a free-fixed or fixed-free lattice corresponding to any other value of δ that is not equal to 0 or ± 1 , a truncation resonance shall appear only if the free end contains the 'lighter' mass, or in other words, a mass less than $m/2$. If such condition is satisfied, the resulting truncation resonance will align perfectly with that of the free-free lattice, assuming a sufficient number of cells allowing this mode to materialize and the deformation profile to exponen-

tially decay from the free end into the bulk of the lattice, effectively not seeing the other (fixed) end. As such, a free-fixed lattice will only have a truncation resonance if $\delta > 0$, while a fixed-free one will only have a truncation resonance if $\delta < 0$.

Diatomic lattice. Consider a diatomic lattice where the spring-mass systems $[m_a, k_a]$ and $[m_b, k_b]$ alternate periodically, with u_i and v_i denoting the displacements of the i^{th} m_a and m_b masses, respectively. Similar to the monatomic lattice, the repeating unit cell can be chosen based on δ , as shown in Fig. 2(a). For any unit cell choice, the motion equations of an isolated diatomic unit cell can be cast as a matrix differential equation: $\mathbf{M}\ddot{\mathbf{z}} + \mathbf{K}\mathbf{z} = \mathbf{f}$, where $\mathbf{z}^T = \{v_i \ u_i \ u_{i+1}\}$, $\mathbf{f}^T = \{0 \ f_L \ f_R\}$, \mathbf{M} is a diagonal matrix of $\{m_b \ m_{a-} \ m_{a+}\}$ where $m_{a\pm} = m_a(1 \pm \delta)/2$, and \mathbf{K} is given by

$$\mathbf{K} = \begin{bmatrix} k_a + k_b & -k_a & -k_b \\ -k_a & k_a & 0 \\ -k_b & 0 & k_b \end{bmatrix} \quad (5)$$

To streamline the analysis, a normalizing frequency ω_0 ,

stiffness contrast ϑ , mass contrast ϱ , and a γ parameter that combines both contrasts are introduced as follows, respectively:

$$\omega_0 = \sqrt{\frac{(k_a + k_b)(m_a + m_b)}{2m_a m_b}} \quad (6a)$$

$$\vartheta = \frac{k_b - k_a}{k_b + k_a} \quad (6b)$$

$$\varrho = \frac{m_b - m_a}{m_b + m_a} \quad (6c)$$

$$\gamma = (1 - \vartheta^2)(1 - \varrho^2) \quad (6d)$$

Both parameters ϑ and ϱ can assume values between -1 and 1 , resulting in $\gamma \in [0, 1]$ for all values of ϱ and ϑ . Upon assuming a harmonic solution and dissolving the internal degree of freedom v_i via Guyan reduction, a transfer matrix equation of the form $\{u_{i+1} \ \epsilon_{i+1}\}^T = \mathbf{T} \{u_i \ \epsilon_i\}^T$ is derived, where $\epsilon_i = f_L/(\omega_0^2 m_a)$ and $\epsilon_{i+1} = -f_R/(\omega_0^2 m_a)$, with the four components of \mathbf{T} being

$$t_{11} = 1 - \frac{2}{\gamma} \left[2 - \delta(1 - \varrho) - \vartheta(1 + \varrho) \right] \Omega^2 + \frac{2}{\gamma} (1 - \delta) \Omega^4 \quad (7a)$$

$$t_{12} = \frac{4}{\gamma} \left[\Omega^2 - (1 - \varrho) \right] \quad (7b)$$

$$t_{21} = \frac{1}{\gamma} \Omega^2 \left[2(1 - \vartheta^2)(1 + \varrho) - (4 - (1 - \varrho)(1 + \delta^2) - 2\delta\vartheta(1 + \varrho)) \Omega^2 + (1 - \delta^2) \Omega^4 \right] \quad (7c)$$

$$t_{22} = 1 - \frac{2}{\gamma} \left[2 + \delta(1 - \varrho) + \vartheta(1 + \varrho) \right] \Omega^2 + \frac{2}{\gamma} (1 + \delta) \Omega^4 \quad (7d)$$

which results in the two following dispersion branches $\Omega = \sqrt{1 \pm \sqrt{1 - \gamma \sin^2(\frac{q}{2})}}$, and a Bragg bandgap sandwiched in between the two limits $\Omega_{\pm} = \sqrt{1 \pm \sqrt{1 - \gamma}}$ with a width of $\Delta\Omega = \sqrt{2 - 2\sqrt{\gamma}}$. As such, a bandgap opens up for all values of $\gamma \neq 1$, with smaller values of γ resulting in larger bandgap widths. Finally, we note that the cut-off frequency of the diatomic lattice remains constant at $\Omega = \sqrt{2}$ regardless of the magnitude of γ .

We focus in the remainder of this discussion on the truncation resonances of the finite diatomic lattice under different boundary conditions, with the understanding that pass-band natural frequencies can always be obtained from \mathbf{T}^n , following the same procedure outlined for the monatomic lattice. As previously established for solid continua, the truncation resonances of a bi-layered phononic crystal with symmetric boundary conditions (e.g., free-free or fixed-fixed) coincide with the natural frequencies of the isolated unit cell itself when subject to the same boundary conditions¹³. As such, the truncation resonances of the free-free diatomic lattice can be

obtained from the roots of Eq. (7c), excluding $\Omega = 0$, resulting a biquadratic equation, from which the following observations can be made:

1. The equation has two positive roots culminating in two truncation resonances: A lower frequency one inside the Bragg bandgap and a higher frequency one above the lattice's cut-off frequency (the latter lies exactly at the cut-off frequency if $\delta = \vartheta$).
2. The equation becomes quadratic when $|\delta| = 1$, since the number of degrees of freedom of the finite lattice reduces by one. The higher frequency truncation resonance ceases to exist (mathematically, it moves to infinity similar to the monatomic lattice case). The lower frequency truncation resonance remains inside the bandgap unless $\varrho = 0$ (zero mass contrast) at which case it moves to one of the two bandgap limits, rendering the lattice free of any bandgap resonances.
3. A perfectly symmetric unit cell ($\delta = 0$) combined with zero stiffness contrast ($\vartheta = 0$) moves

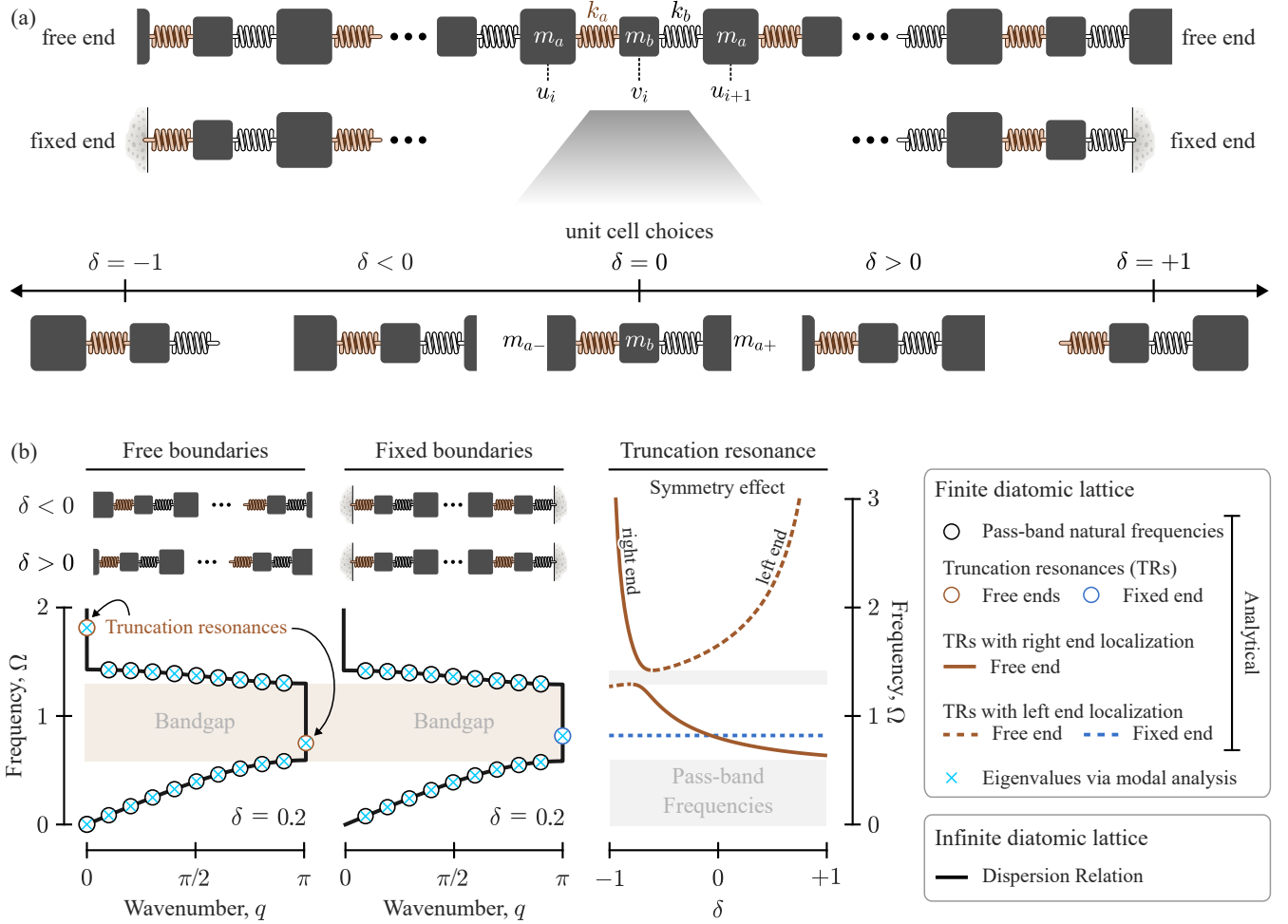


FIG. 2. **Diatomic lattice.** (a) Schematic diagram of a finite diatomic lattice comprised of a series of alternating masses $m_{a,b}$ connected via alternating springs $k_{a,b}$, subject to free and fixed boundary conditions. Owing to its periodicity, the building block (unit cell) of the diatomic lattice can be defined in an infinite number of ways using the single symmetry parameter δ , where $-1 \leq \delta \leq 1$, which dictates the values of m_{a+} and m_{a-} (together forming the lumped mass m_a) which sit on either side of the intermediate mass m_b . While the choice of unit cell does not affect the dispersion relation, a finite lattice shall generally have different end masses whose values depend on the sign and value of δ . A positive δ will result in a heavier portion of the lumped mass ($> m_a/2$) on the right end of the lattice, and vice versa. A zero value of δ denotes a perfectly symmetric unit cell where $m_{a+} = m_{a-} = m_a/2$. (b) Natural frequencies of a free-free (left) and fixed-fixed (middle) finite diatomic lattice of $n = 10$ unit cells, $\delta = 0.2$, $\varrho = 1/3$, and $\vartheta = -3/5$, superimposed on the dispersion diagram of the infinite lattice. Truncation resonances (TRs) are marked with a circular marker of different color for distinction. Two TRs appear in the free-free lattice at $\Omega = 0.742, 1.796$ while one exists in the fixed-fixed case at $\Omega = 0.817$. The rightmost plot tracks the location of the aforementioned TRs as δ varies, showing critical unit cell configurations at which the localization edge shifts from one side of the free-free diatomic lattice to the other, and confirms the indifference of the fixed-fixed TR to the unit cell choice.

the lower frequency truncation resonance to the bandgap limit located at $\Omega = \sqrt{1 + \varrho}$, which could be either the lower or upper limit depending on the sign of ϱ .

The leftmost panel of Fig. 2(b) shows the dispersion diagram of a diatomic lattice with a unit cell configuration corresponding to $\delta = 0.2$, and mass and stiffness contrasts of $\varrho = 1/3$ and $\vartheta = -3/5$, respectively. Since it consists of a repeated array of two degree-of-freedom unit cells, the diatomic lattice has two wave modes described by an acoustic (lower) and an optical (upper) branches which sit on both ends of the Bragg bandgap. Shown in the same figure are the $2n + 1 = 21$ natural frequen-

cies of a finite free-free diatomic lattice constructed from $n = 10$ unit cells of the same configuration, confirming the two truncation resonances stated in observation #1, one falling inside the bandgap at $\Omega = 0.742$ and the other taking place above the optical branch at $\Omega = 1.796$.

The fixed-fixed diatomic lattice has a single truncation resonance at $\Omega = \sqrt{1 - \varrho}$, representing the positive root of Eq. (7b), and shows, once again, independence of the symmetry parameter δ . The edge mode profile accompanying this truncation resonance exhibits localized displacement at the stiffer end of the lattice. In other words, the localization takes place at the right end if the contrast ϑ is positive and vice versa. Interestingly, in the case of $\varrho = 0$, the truncation resonance occurs at a con-

stant frequency of $\Omega = 1$ regardless of the stiffness contrast ϑ , a feature which has been exploited in diatomic lattices with topological protection²⁵. The middle panel of Fig. 2(b) displays the behavior of the finite fixed-fixed diatomic lattice and confirms the presence of a sole truncation resonance inside the bandgap at $\Omega = 0.817$ for the same values of ϱ and ϑ used in the free-free example.

Finally, given the dependence of both truncation resonances of the free-free diatomic lattice on δ , it is important to highlight this effect of unit cell symmetry on the edge mode profile associated with each of these two resonances, which is succinctly captured by the rightmost plot Fig. 2(b). As can be seen, there exists a critical value of δ for each truncation resonance at which that particular resonance touches the lattice's pass-band regions, and at which the end of the lattice which exhibits the localized displacement shifts from the one side to the other, a behavior which has been similarly observed in recent studies^{8,13}. Consistent with the earlier hypothesis, the same plot shows a flat line tracking the location of the fixed-fixed truncation resonance with a varying δ , confirming the lack of a symmetry effect for that system.

Acknowledgements. The authors acknowledge support of this work by the US National Science Foundation through research awards no. 1847254 (CAREER) and 1904254, and the US Air Force Office of Scientific Research through award no. FA9550-23-1-0564.

- ¹M. M. Sigalas, "Elastic and acoustic wave band structure," *Journal of sound and vibration* **158**, 377–382 (1992).
- ²M. M. Sigalas and E. N. Economou, "Comment on acoustic band structure of periodic elastic composites," *Physical Review Letters* **75**, 3580 (1995).
- ³M. I. Hussein, M. J. Leamy, and M. Ruzzene, "Dynamics of phononic materials and structures: Historical origins, recent progress, and future outlook," *Applied Mechanics Reviews* **66**, 040802 (2014).
- ⁴T. Vasileiadis, J. Varghese, V. Babacic, J. Gomis-Bresco, D. Navarro Urrios, and B. Graczykowski, "Progress and perspectives on phononic crystals," *Journal of Applied Physics* **129** (2021).
- ⁵H. Al Ba'ba'A and M. Nouh, "An investigation of vibrational power flow in one-dimensional dissipative phononic structures," *Journal of Vibration and Acoustics, Transactions of the ASME* **139**, 21003–21010 (2017).
- ⁶S. Roman and D. H. Sebastian, "Observation of phononic helical edge states in a mechanical topological insulator," *Science* **349**, 47–50 (2015).
- ⁷E. Prodan, K. Dobiszewski, A. Kanwal, J. Palmieri, and C. Prodan, "Dynamical Majorana edge modes in a broad class of topological mechanical systems," *Nature Communications* **8** (2017), 10.1038/ncomms14587.
- ⁸M. I. Rosa, R. K. Pal, J. R. Arruda, and M. Ruzzene, "Edge States and Topological Pumping in Spatially Modulated Elastic Lattices," *Physical Review Letters* **123**, 034301 (2019).
- ⁹M. I. Hussein, S. Biringen, O. R. Bilal, and A. Kucala, "Flow stabilization by subsurface phonons," *Proceedings of the Royal Society A: Mathematical, Physical and Engineering Sciences* **471**, 20140928 (2015).
- ¹⁰S. Balasubramanian, S. Park, K. Matlack, and A. Goza, "Harnessing phononic materials for aerodynamic flow control," in *AIAA AVIATION 2022 Forum* (2022) p. 3240.
- ¹¹C. J. Barnes, C. L. Willey, K. Rosenberg, A. Medina, and A. T. Juhl, "Initial computational investigation toward passive transition delay using a phononic subsurface," in *AIAA Scitech 2021 Forum* (2021) p. 1454.
- ¹²B. L. Davis, A. S. Tomchek, E. A. Flores, L. Liu, and M. I. Hussein, "Analysis of periodicity termination in phononic crystals," in *ASME International Mechanical Engineering Congress and Exposition*, Vol. 54945 (2011) pp. 973–977.
- ¹³H. B. Al Ba'ba'a, C. L. Willey, V. W. Chen, A. T. Juhl, and M. Nouh, "Theory of truncation resonances in continuum rod-based phononic crystals with generally asymmetric unit cells," *Advanced Theory and Simulations* **6**, 2200700 (2023).
- ¹⁴M. I. Rosa, B. L. Davis, L. Liu, M. Ruzzene, and M. I. Hussein, "Material vs. structure: Topological origins of band-gap truncation resonances in periodic structures," *Physical Review Materials* (2023).
- ¹⁵L. Sangiuliano, C. Claeys, E. Deckers, and W. Desmet, "Influence of boundary conditions on the stop band effect in finite locally resonant metamaterial beams," *Journal of Sound and Vibration* **473**, 115225 (2020).
- ¹⁶X.-F. Lv, X. Fang, Z.-Q. Zhang, Z.-L. Huang, and K.-C. Chuang, "Highly localized and efficient energy harvesting in a phononic crystal beam: Defect placement and experimental validation," *Crystals* **9**, 391 (2019).
- ¹⁷L. Katch, M. Moghaddaszadeh, C. Willey, A. Juhl, M. Nouh, and A. Argüelles, "Analysis of geometric defects in square locally resonant phononic crystals: A comparative study of modeling approaches," *The Journal of the Acoustical Society of America* **154**, 3052–3061 (2023).
- ¹⁸T.-C. Wu, T.-T. Wu, and J.-C. Hsu, "Waveguiding and frequency selection of lamb waves in a plate with a periodic stubbed surface," *Physical Review B* **79**, 104306 (2009).
- ¹⁹M. Oudich, B. Djafari-Rouhani, B. Bonello, Y. Pennec, and F. Sarry, "Phononic crystal made of multilayered ridges on a substrate for rayleigh waves manipulation," *Crystals* **7**, 372 (2017).
- ²⁰H. Al Ba'ba'a, M. Nouh, and T. Singh, "Pole distribution in finite phononic crystals: Understanding Bragg-effects through closed-form system dynamics," *The Journal of the Acoustical Society of America* (2017), 10.1121/1.5001513.
- ²¹H. Al Ba'ba'a, M. Nouh, and T. Singh, "Dispersion and topological characteristics of permutative polyatomic phononic crystals," *Proceedings of the Royal Society A: Mathematical, Physical and Engineering Sciences* **475** (2019), 10.1098/rspa.2019.0022.
- ²²H. Al Ba'ba'a, D. Depauw, T. Singh, and M. Nouh, "Dispersion transitions and pole-zero characteristics of finite inertially amplified acoustic metamaterials," *Journal of Applied Physics* **123**, 105106 (2018).
- ²³M. V. Bastawrous and M. I. Hussein, "Closed-form existence conditions for bandgap resonances in a finite periodic chain under general boundary conditions," *The Journal of the Acoustical Society of America* **151**, 286–298 (2022).
- ²⁴Y.-K. Lin and T. McDaniel, "Dynamics of beam-type periodic structures," *Journal of Engineering for Industry* (1969), <https://doi.org/10.1115/1.3591761>.
- ²⁵H. Chen, H. Nassar, and G. L. Huang, "A study of topological effects in 1D and 2D mechanical lattices," *Journal of the Mechanics and Physics of Solids* **117**, 22–36 (2018).